THE ASTROPHYSICAL JOURNAL, 426:109–115, 1994 May 1

IRAS COLORS WITHIN M31: EVIDENCE FOR DEFICIENCY OF VERY SMALL GRAINS?

CONG XU
Max-Planck-Institut für Kernphysik, Postfach 103980, W6900 Heidelberg, Germany; also
Max-Planck-Institut für Radioastronomie, Bonn, Germany

AND

GEORGE HELOU
IPAC 100-22, California Institute of Technology, Pasadena, CA 91125
Received 1993 September 13; accepted 1993 November 4

ABSTRACT

Significant differences are found in the *IRAS* color-color diagrams of small regions (2′ × 2′, or 0.4 × 1.8 kpc) within the disk of M31 compared to Galactic cirrus, most noticeably demonstrated by a trend of low 60 to 100 μm surface brightness ratio and high 12 to 25 μm ratio. Based on physical arguments, we conclude that these color differences are best explained by assuming that "very small grains" (but not polycyclic aromatic hydrocarbons) are only half as abundant in M31 as they are in Galactic cirrus. We confirm this conclusion and test its detailed agreement with data by using the phenomenological model of Désert et al. (1990). In particular, we show that the data cannot be explained by postulating weaker UV heating in the disk of M31. We also show that the VSG-deficient model predicts correctly the correspondence between the *IRAS* colors and the 100 μm emissivity per H I atom in the outer disk of M31.

"Very small grains" are a leading candidate for the carrier of the 2175 Å bump in the extinction curve. Our suggested VSG deficiency in M31 is thus consistent with recent *HST* observations which show evidence for a weaker and narrower 2175 Å bump on the M31 extinction curve. Some speculation is offered as to possible links between very small grains and the low rate of current star formation in M31.

Subject headings: dust, extinction — galaxies: individual (M31) — galaxies: ISM — infrared: ISM: continuum

1. INTRODUCTION

It is now widely accepted that small grains ($\lesssim$100 Å) are an important ingredient of interstellar dust (Puget & Léger 1989). Accurate determinations of the ultraviolet (UV) extinction curve toward a variety of stars using the *International Ultraviolet Explorer* (see Mathis 1990 for a review) revealed that the extinction cross section of dust keeps rising from the optical toward the UV, with a "bump" near 2175 Å, and a nonlinear rise in the far-UV ($\lambda \geq 2000$ Å). This behavior cannot be attributed to large grains ($\gtrsim$100 Å) which, because of their large size, contribute mainly to the near-infrared and optical extinction (Draine & Lee 1984). Near-infrared and mid-infrared spectroscopic studies of a wide variety of objects (H II regions, reflection nebulae, planetary nebulae, interstellar cirrus, and galaxies) revealed a set of emission features at 3.3, 6.2, 7.7, 8.6, and 11.3 μm, which have been successfully associated with polycyclic aromatic hydrocarbon molecules (PAH) by Léger & Puget (1984; see also Puget & Léger 1989). These are two-dimensional molecules of $\sim$10 Å in size, which are heated by a single photon to more than 1000 K and then reemit the energy mostly in the "aromatic" infrared features. Empirical arguments (Helou, Ryter, & Soifer 1991) and model calculations have suggested that they dominate the 12 μm *IRAS* flux of various objects including galaxies (Xu & De Zotti 1989).

These PAHs, however, have difficulty accounting for the diffuse 25 μm radiation seen in the solar neighborhood (Boulanger & Pérault 1989), in the Galactic plane (Cox & Mezger 1988; Pérault et al. 1988), and in nearby galaxies such as M31 (Walterbos & Schwering 1987), without getting uncomfortably large (well over 1000 carbon atoms), and losing their PAH character (Désert et al. 1990, hereafter DBP90). Large grains in thermal equilibrium on the other hand cannot account for the diffuse 25 μm emission because they are too cool ($\sim$20 K; Draine & Anderson 1985). Désert et al. (1990) therefore suggested a population of three-dimensional very small grains (VSG) of size 10–150 Å as the predominant source for the diffuse 25 μm radiation. Similar to PAHs, VSG undergo significant temperature fluctuations when heated by optical or UV radiation, but reemit the energy in the mid-infrared continuum rather than in features. These VSG will in addition contribute to the 60 μm diffuse radiation, a desirable feature in view of the constant 60 μm to 100 μm flux ratio in the Galactic plane (Cox & Mezger 1988; Pérault et al. 1988) and in the disk of M31 (Walterbos & Schwering 1987). This constancy is reproduced by the combination of VSG and large grains but is quite unlikely behavior for large grains alone whose temperatures must decrease substantially from inner to outer disk with the decrease of the radiation field (Helou 1989).

While the properties of PAH molecules have been well studied both astronomically and in the laboratory, very few studies in the literature have been devoted to VSG, and these studies have been exclusively confined to Galactic objects (Sellgren 1984; Castelaz, Sellgren, & Werner 1987; Draine & Anderson 1985; DBP90). This is basically due to the difficulty of spectroscopic measurements beyond 20 μm, where VSG emit most of their radiation. For galaxies outside the Milky Way, there is the additional obstacle that the total fluxes at 25 μm and at 60 μm are very often dominated by the warm dust associated with star formation regions (Xu & de Zotti 1989; Rice et al. 1990), so that information about the VSG in the diffuse medium is effectively masked. Consequently, little is known about the nature of VSG. The small graphite grain

hypothesis has been favored by many authors because these same grains are strong candidates for providing the 2175 Å bump in the UV extinction curve (DBP90; Mathis 1990). It is completely unclear, however, where and how VSG form, and what determines the abundance of VSG relative to "classical" large grains. Helou et al. (1991) have shown that the abundance of PAHs relative to large grains is constant with a rms dispersion of about 40% among galaxies; however, the question of VSG abundance variations from galaxy to galaxy has not been addressed.

We report here on a study of the *IRAS* colors of small areas a few hundred pc in size within the disk of M31. This galaxy is perhaps the best target for studying VSG outside the Milky Way using *IRAS* data, because (1) it is the nearest spiral galaxy outside the Milky Way, and thus it is well resolved by *IRAS*; (2) it is a well-known quiescent galaxy (Walterbos 1987), and therefore at 60 μm and even 25 μm, the emission is still dominated by the diffuse dust *not* associated with the star formation regions. The study uses new high-resolution ($\sim 1'$) *IRAS* maps. We find the *IRAS* color-color diagram of the diffuse emission of M31 to be unusual compared to Galactic cirrus, showing a trend of having rather low 60 to 100 μm surface brightness ratios and high 12 to 25 μm ratios. This observation can be most naturally explained by a deficiency of VSG in M31. Throughout this paper, we assume for M31 a distance of 690 kpc ($1' = 200$ pc along the major axis), an inclination angle of 77°, and P.A. = 37°.

2. THE DATA

The new high-resolution *IRAS* maps at 12, 25, 60, and 100 μm were obtained from the high-resolution processor (HiRes) developed at the Infrared Processing and Analysis Center (IPAC) and based on the maximum correlation method described by Aumann, Fowler, & Melnyk (1990). The resolution achieved in these maps is $\sim 0.'5 \times 0.'9$ (in-scan and cross-scan half-power diameters, respectively) for the 12 and 25 μm maps, $\sim 0.'8 \times 1'$ for the 60 μm map, and $\sim 1.'5 \times 1.'5$ for the 100 μm map. However, the resolution is not uniform over the maps (Fowler & Aumann 1993) and depends in particular on the surface brightness of the background. In order to overcome this problem, and also to simplify the comparison between the four maps, we smooth all of them to a 1.'7 circular beam on a grid with 0.'5 pixels. Furthermore, the quantitative analysis in this paper is carried out on a sample of small areas ("cells"), rather than pixels, each of size $2' \times 2'$. The surface brightness at wavelength λ ($\lambda = 12$, 25, 60, and 100 μm), $I_\nu(\lambda)$ in Jy sr^{-1}, of each cell is calculated from the corresponding smoothed map by averaging the surface brightness of a 4×4 array of adjacent pixels. These precautions should have essentially removed the problem of ununiform resolutions of the HiRes maps (J. W. Fowler, private communication).

Several versions of reduced *IRAS* data on M31 have been published, reporting a variety of values for its total integrated fluxes, as shown in Table 1. While we are more concerned with the surface brightness distribution than with the total flux, this is the simplest way to compare the various data sets. The first three sets of numbers are reproduced from the listed references, while the fourth set was measured from the *IRAS* Sky Survey Atlas (ISSA) using the same method that we used to extract total fluxes from the HiRes maps. The method consisted of estimating the local background sky brightness in about 20 circular areas of 10′ radius, verifying that these estimates were consistent with a constant background, removing the latter, then spatially integrating the emission from the galaxy. The sources of the uncertainty of M31 integrated fluxes calculated in this work are discussed in Appendix.

There is substantial discrepancy between the various determinations of the M31 fluxes, reflecting primarily improvements in data processing techniques, and small revisions to the calibration of *IRAS* data. Our HiRes data show very good agreement with ISSA at 60 and 100 μm, but run larger than ISSA by about 25% at 12 and 25 μm, signaling a possible calibration error. Although the astronomical result we report in this paper is based mainly on the deficiency of 60 μm emission related to 100 μm emission, which is not affected by the discrepancy found here, it also involves, to some extent, the excess surface brightness at 25 μm relative to 60 μm, which has the same sign as the discrepancy of HiRes fluxes compared to ISSA fluxes. However, the magnitude of this discrepancy is too small to affect our main conclusions significantly.

3. *IRAS* COLOR-COLOR DIAGRAMS

With the four *IRAS* bands one can construct maximally three *independent* flux ratios ("colors"), for which we choose $R(12, 25) = I_\nu(12\ \mu m)/I_\nu(25\ \mu m)$, $R(25, 60) = I_\nu(25\ \mu m)/I_\nu(60\ \mu m)$, and $R(60, 100) = I_\nu(60\ \mu m)/I_\nu(100\ \mu m)$. *IRAS* color-color diagrams are powerful tools for studying both the grain composition (PAH, VSG, silicate, graphite, etc.) and the heating process of dust in different environment (e.g., in star formation regions or in quiescent interstellar space). Helou (1986) suggested a two-component model which interprets the anticorrelation between $R(60, 100)$ and $R(12, 25)$ of *galaxies* as resulting from the superposition of two components of FIR emission from interstellar dust: a warm component with high $R(60, 100)$ and low $R(12, 25)$, and a cool component with low $R(60, 100)$ and high $R(12, 25)$. The warm component is in general associated to massive star formation regions, while the cool component is associated with "cirrus" or with quiescent molecular clouds heated by the interstellar radiation field (ISRF). Xu & De Zotti (1989) associated this model with a more realistic grain model which includes PAHs and applied it to the $R(60, 100)$ versus $R(12, 25)$ diagrams and $R(60, 100)$

TABLE 1

TOTAL FLUXES OF M31 REDUCED *IRAS* DATA

Reference	$f_\nu(12\ \mu m)$	$f_\nu(25\ \mu m)$	$f_\nu(60\ \mu m)$	$f_\nu(100\ \mu m)$
Walterbos & Schwering 1987	175 ± 10	150 ± 5	610 ± 5	2850 ± 100
Rice et al. 1988	163	108	536	2928
Rice et al. 1993	135	99	496	2507
ISSA 1993	172	146	619	3223
This work 1994	217 ± 52	183 ± 38	615 ± 29	3089 ± 309

versus $R(25, 60)$ diagrams of both star-forming galaxies (Markarian galaxies) and normal spiral galaxies. Sauvage, Thuan, & Vigroux (1990) showed, in the case of the Magellanic Clouds, that the two-component model also applies to regions within galactic disks.

We study the *IRAS* color-color diagrams of a complete sample of small cells in M31. Each cell, 2′ × 2′ in size, corresponds to a small region of 0.4 kpc × 1.8 kpc in the M31 disk. We have included only those cells which are within 80′ from the center in the plane of M31 ($r \leq 16$ kpc for the assumed distance of 690 kpc). We consider only cells with surface brightness sufficiently high that each of the *IRAS* color ratios plotted in the following figures is significant at least at the 3 σ level.

In Figure 1 is plotted the color-color diagram $R(60, 100)$ versus $R(12, 25)$ for the M31 cells. The plus signs show the colors of the bulge region, a central elliptical area of 20′ × 12′ (Walterbos & Kennicutt 1988), which is warmer in emission compared to the disk in both $R(60, 100)$ and $R(12, 25)$. Soifer et al. (1987) have found that the 12 and 25 μm emission of the M31 bulge includes a substantial contribution from circumstellar envelopes around evolved low-mass stars, which is perhaps never significant in galactic disks. On the other hand, the 60 and 100 μm fluxes of the bulge are likely due to interstellar dust heated by the intense ISRF supplied primarily by old stars.

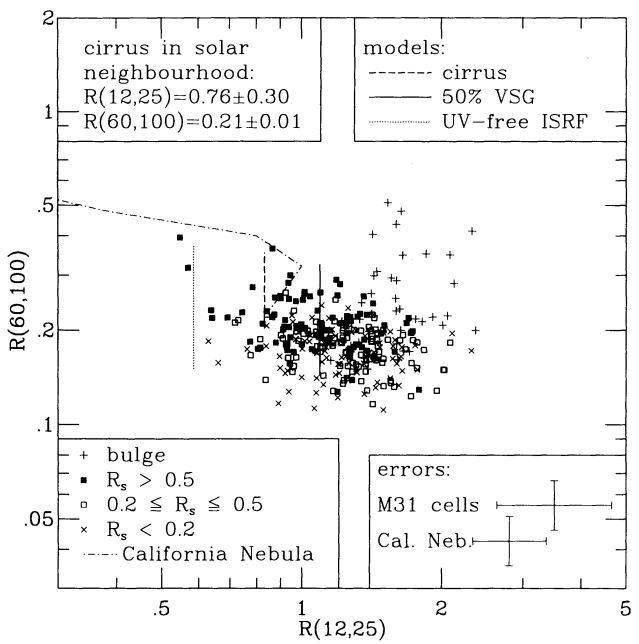

FIG. 1.—$R(60, 100)$ vs. $R(12, 25)$ diagram for cells (2′ × 2′) in M31. The plus signs are cells in the bulge region. Other points are cells in the disk: solid squares are those with significant contribution from sources [$R_s = f_\nu^s(60\ \mu m)/f_\nu(60\ \mu m) > 0.5$], open squares are those with intermediate R_s ratio ($0.2 \leq R_s \leq 0.5$), and the crosses are dominated by the diffuse emission ($R_s < 0.2$). For comparison, the corresponding ratios of the cirrus in solar neighborhood is given in the upper right-hand corner of the figure. The dashed-dotted line is the color sequence of the California nebula (Boulanger et al. 1988), which goes from the center of the star-forming region (the upper left-hand corner of the figure) to the outer part of the nebula. Galaxies are usually located near this line. The dashed vertical line is the model prediction by Désert et al. (1990) for the Galactic cirrus. The range of the intensity of ISRF in the model calculation is 0.05–10 times that of in the solar neighborhood. The dotted line is the prediction of the same dust model but heated by an ISRF without any UV light. The solid line is the prediction from a model which is otherwise the same with that of Désert et al. (1990), but the abundance of very small grains (VSG) is multiplied by a factor of 0.5.

The other points in Figure 1 show the disk colors, with various symbols indicating different significance of the contribution from the dust associated with star formation regions (the warm component), which is estimated from the ratio

$$R_s = f_\nu^s(60\ \mu m)/f_\nu(60\ \mu m)\ , \qquad (1)$$

where $f_\nu^s(60\ \mu m)$ is the 60 μm flux due to the discrete sources in a cell in question, and $f_\nu(60\ \mu m)$ its total 60 μm flux. The sources, which are exclusively related to giant H II regions or H II region complexes (Rice et al. 1990; Xu et al. 1992), are extracted from the 60 μm map using Gaussian fittings. It is argued that the radiation from these sources represents well the warm component (Xu & Helou 1994). As explained in the legend, the solid squares represent the regions where the warm component dominates ($R_s > 0.5$), the crosses, the regions where the warm component is diminishing ($R_s < 0.2$), and the open squares, the cells in the intermediate situation.

The dash-dotted line is the *IRAS* color sequence of the California nebula measured by Boulanger et al. (1988), stretching from the most intensely heated region (the upper left-hand corner of Fig. 1) to the cooler outer parts of the nebula. The distribution of galaxies on the same color-color diagram generally follows this sequence (Boulanger et al. 1988; Helou 1989). The dashed vertical line shows the colors calculated by DBP90 for Galactic cirrus using the three-population dust model with PAHs, VSG, and large grains. The color variation along the line reflects a range in the intensity of the heating radiation from 0.05 to 10 times the ISRF in the solar neighborhood. The line is vertical because in the DBP90 model the spectral shapes of PAH and VSG emission and their relative intensity are almost independent of the intensity of heating radiation.

There is a clear trend in this diagram that cells with larger R_s ratios show warmer $R(60, 100)$ *and* cooler $R(12, 25)$ ratios. This is in good agreement with the two-component model (Helou 1986). It should be pointed out that the data points in the bulge do not follow the two-component model, simply because the mechanism of the MIR-FIR emission there is somewhat different. However, it contributes so little (~10%) to the integrated emission of M31 that the validity of the two-component model for the global colors of normal spiral galaxies is not affected.

On the other hand, most of the emission in the M31 disk, especially that from the cells with little contribution from the sources (*crosses*), has cooler $R(60, 100)$ and warmer $R(12, 25)$ ratios than the cirrus in the solar neighborhood [$R(60, 100) = 0.21 \pm 0.01$ and $R(12, 25) = 0.76 \pm 0.30$; Boulanger & Pérault 1988]. This cannot be due to the difference in the intensity of ISRF because the entire trajectory of the cirrus model (*dashed line*) which spans a very wide range of ISRF intensity (0.05–10 times of the local ISFR), lies near the left-hand border of the data domain.

The problem is presented even better in the $R(60, 100)$ versus $R(25, 60)$ diagram which is plotted in Figure 2. Cells in the bulge have been excluded to simplify the plot. The points are coded by the ratio R_s as in Figure 1. The dashed-and-dotted curve again represents the color sequence of the California nebula. The dashed line is the DBP90 model prediction for Galactic cirrus, with lower $R(25, 60)$ corresponding to more intense heating. Cirrus colors as observed in the solar neighborhood (Boulanger & Pérault 1988) occur near the minimum of this curve. Clearly, this color-color diagram allows better discrimination at lower heating intensities than Figure 1, with

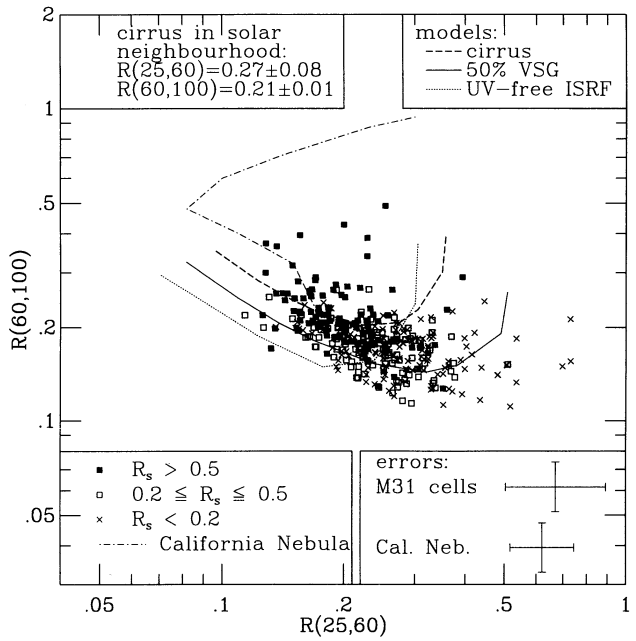

FIG. 2.—R(60, 100) vs. R(25, 60) diagram for cells (2′ × 2′) in M31 disk. Cells in the bulge regions (Fig. 1, *plus signs*) have been deliberately excluded. Other symbols have the same meaning as in Fig. 1.

the points separating out in R_s ratio, and spreading out in a weak anticorrelation R(60, 100) versus R(25, 60). The data, especially those for the cells with little contribution from the sources (*crosses*), are clearly inconsistent with the model prediction for Galactic cirrus.

4. INTERPRETATION

4.1. *Physical Argument*

The diffuse emission from the disk of M31, represented by the cells of $R_s < 0.2$, displays *IRAS* colors which are different from Galactic cirrus: the mean R(60, 100) of these cells, 0.167 ± 0.003, is significantly lower than the ratio R(60, 100) = 0.21 ± 0.01 for the cirrus in the solar neighborhood (Boulanger & Pérault 1988), and the mean R(12, 25) = 1.23 ± 0.03 is significantly higher than that of the solar neighborhood cirrus. In the R(60, 100) versus R(25, 60) diagram, many of these cells show high 25-to-60 μm surface brightness ratios (>0.5) and low 60 to 100 μm surface brightness ratios (<0.2) at the same time. The mean R(25, 100) = 0.047 ± 0.002 of cells with $R_s < 0.2$ is slightly lower than that of the solar neighborhood cirrus.

The constant R(60, 100) in the diffuse emission in the Milky Way is interpreted as due to the contribution of emission from "very small grains" (VSG) (Cox & Mezger 1988; Pérault et al. 1988), whose contribution determines the minimum R(60, 100) reached at low radiation densities. The unusually low R(60, 100) values in the diffuse medium of M31 must therefore indicate a deficiency in VSG emission. This might reflect either a lack of UV heating (Milliard 1984) that drives VSG fluctuations, or a lack of VSG.

A weak UV radiation field would depress even more noticeably the 12 μm emission, because the latter is due primarily to PAHs which are more efficient than VSG at absorbing far UV photons. Since the 12 μm emission is *not* depressed (relative to 100 μm) in the M31 regions in question, a weak UV field is an unlikely hypothesis.

On the other hand, VSG can be heated to relatively high temperatures (~a few hundred kelvin; Draine & Anderson 1985) by a single UV or optical photon. They are therefore likely to be the most important contributors to the diffuse (cirrus) 25 μm emission as well as the 60 μm emission in regions of low radiation density. It would therefore seem that the more natural explanation of the *IRAS* colors of M31 cirrus is a deficiency in VSG compared to normal large grains and PAHs.

It should be noted, however, that the integrated *IRAS* colors of M31, calculated from the fluxes in Table 1, do not indicate compellingly a VSG-deficient ISM, probably because the evidence is masked by the superposed emissions from various dust populations (e.g., the diffuse dust in the disk and the dust associated to the star formation regions) at different heating intensities.

In what follows, we will use the phenomenological dust model of Désert et al. (1990) to clarify and illustrate the above arguments and verify the detailed agreement between the data and our conjecture.

4.2. *Model Comparison*

In Figures 1 and 2, the dotted line shows the prediction by the DBP90 model, when dust is heated by a solar neighborhood ISRF with the UV light removed, scaled in intensity by a factor varying from 0.05 to 10. This UV-free model fails to reproduce the data, primarily because it predicts too low a R(12, 25) ratio in Figure 1, as might be expected since the UV photons would have provided the greater temperature fluctuations (in both VSG and PAH), and the associated warmer mid-infrared emission. In Figure 2, the UV-free model predicts too low a value of R(25, 60), because both PAH and VSG emissivity drops, affecting the flux at 25 μm slightly more than the flux at 60 μm, which still gets contribution from the large grains.

The solid lines in Figures 1 and 2 show the prediction by the DBP90 model modified by reducing the VSG abundance to half its value in Galactic cirrus. This variation on the model provides the best fit to the data. R(60, 100) is reduced because of a smaller contribution from VSG to I_ν(60 μm), whereas R(12, 25) is enhanced because of the increased abundance of PAHs relative to VSG, in agreement with the data in Figure 1. As the intensity of the heating radiation drops below the solar neighborhood value, large grains cool down, so their reduced contribution at 60 μm causes the increased R(25, 60) values, thus aligning model predictions and data in Figure 2. At the lowest heating levels the large grains are so cold that their emissivity at 100 μm drops enough to cause the upturn in the solid line on Figure 2.

In Figure 3 we extend the testing of the VSG-deficient model by examining the emissivity per H I atom. We plot R(60, 100) versus R(25, 60) for cells outside the well-known bright ring ($7 \lesssim r \lesssim 12$ kpc), i.e., cells in the annulus $12 \leq r \leq 14.5$ kpc; outside of 14.5 kpc, the signal-to-noise ratio drops below 3 everywhere. This annulus offers a reasonably broad range of heating intensities but remains sufficiently narrow to avoid potential effects due to radial gradients in metallicity and dust-to-gas ratios (Walterbos & Kennicutt 1988). The conditions for dust emission in star-formation regions are very different from those for diffuse dust emission, thus we exclude the cells with $R_s > 0.5$ in order to concentrate on the diffuse dust emission. The points in Figure 3 are marked according to E(100, H I) = $\bar{I}_\nu(100\ \mu\text{m})/N_{\text{H I}}$ ratio in units of MJy sr^{-1}/10^{20} H cm^{-2}: solid squares are cells with E(100, H I) > 0.4, open squares are cells

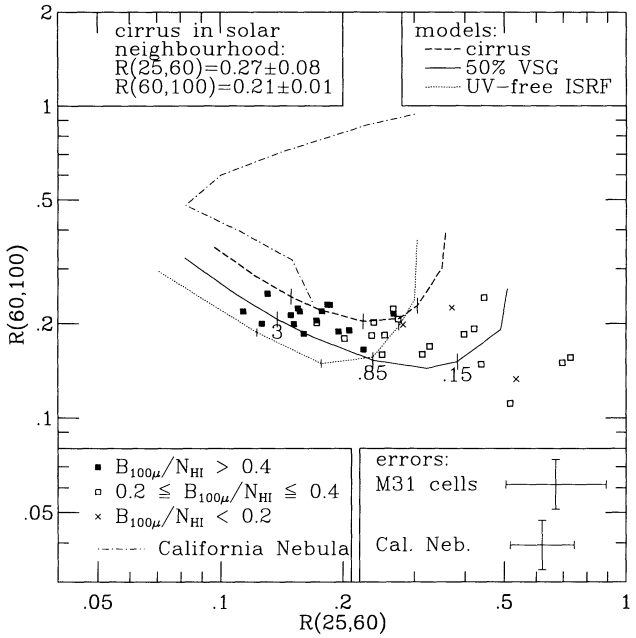

FIG. 3.—$R(60, 100)$ vs. $R(25, 60)$ diagram for cells (2′ × 2′) in M31 outer disk ($12 \leq r \leq 14.5$ kpc). Only cells with $R_s \leq 0.5$ are included. They are marked according to the $I_\nu(100\ \mu m)/N_{H\,I}$ ratio: solid squares are those with $I_\nu(100\ \mu m)/N_{H\,I} > 0.4$(MJy sr^{-1}/$10^{20}$ H cm^{-2}), open squares are those with $0.2 \leq I_\nu(100\ \mu m)/N_{H\,I} \leq 0.4$(MJy sr^{-1}/$10^{20}$ H cm^{-2}), and crosses are those with $I_\nu(100\ \mu m)/N_{H\,I} < 0.2$(MJy sr^{-1}/$10^{20}$ H cm^{-2}). Other symbols have the same meanings as in Fig. 2. The three numbers (0.15, 0.85, 3) along the solid line give the $I_\nu(100\ \mu m)/N_{H\,I}$ values in units of MJy sr^{-1}/10^{20} H cm^{-2}, predicted by the model at the corresponding positions on that line assuming a local dust-to-gas ratio (Désert et al. 1990). Tick marks on the other two model lines correspond to the same $I_\nu(100\ \mu m)/N_{H\,I}$ values.

with $0.2 \leq E(100, H\ I) \leq 0.4$; and crosses the cells with $E(100, H\ I) < 0.2$. The cirrus in the solar neighborhood has $E(100, H\ I) = 0.85 \pm 0.03$ in the same units (Boulanger & Pérault 1988). Other symbols have the same meanings as in Figure 2. The three numbers (0.15, 0.85, 3) along the solid line give the values of $E(100, H\ I)$, as predicted by the model at the corresponding positions on that line, assuming a solar neighborhood dust-to-gas ratio (DBP90). There are also corresponding tick marks on the dotted line (the cirrus model) and the dashed line (the UV-free model).

The VSG-deficient model (Fig. 3, *solid line*) fits the data much better than the other two models, namely standard and UV-free Galactic cirrus. In the diagram, the low-$E(100, H\ I)$ points (*open squares* and *crosses*), and the high-$E(100, H\ I)$ points (*solid squares*) are well separated as anticipated from the model. However, the boundary between the two sets of points occurs where the model predicts $E(100, H\ I) \sim 0.85$ rather than ~ 0.4 as required by the measurements. This is likely due to a dust-to-gas ratio which is depressed in the outer disk of M31 compared to the solar neighborhood which was used as the basis of the DBP90 model (Walterbos & Kennicutt 1988). A dust-heating model (Xu & Helou 1994), which makes use of available UV, optical, and H I maps, and which fits well the spatial distribution of FIR surface brightness in M31, confirms that the dust–to–H I gas ratio at a galactocentric distance of ~ 14 kpc is about a factor of 2 lower than the solar neighborhood value, just as required by the data.

We therefore conclude that the data are compatible with the model predictions of DBP90 assuming that the VSG abundance relative to large grains and PAHs in M31 is only one-half of its value in the local Milky Way.

5. DISCUSSION

We find a significant difference in the *IRAS* colors of the diffuse dust emission of M31 compared to the large-scale emission (cosecant law) in the solar neighborhood. The difference cannot be reproduced by the DBP90 model assuming UV-deficient heating of the dust in M31. It can be explained however by the same model assuming a VSG abundance half of that in the solar neighborhood. This assumption also predicts the locations in the *IRAS* color-color diagrams of cells in the outer regions of the M31 disk with low- and high-$I_\nu(100\ \mu m)/N_{H\,I}$ values. While the modeling works consistently for all M31 cells, the effect is most obvious where the radiation field is the weakest.

The VSG deficiency in M31 would remain a model-dependent result if based solely on the *IRAS* data, since no direct VSG signature is involved, and DBP90 may have oversimplified PAH and VSG properties, especially at low heating levels. One hint to this effect is that the model tends to predict an overabundance of VSG at high radiation densities, as evident in Figures 10 and 11 of DBP90. However, a strong independent argument in favor of the VSG deficiency would be provided by a weaker 2175 Å bump, in line with the suggestion (Mathis 1990) that VSG are responsible for the bump. Recent *HST* data do indeed reveal narrower and weaker 2175 Å bumps in the extinction spectra derived for two stars at opposite sides of M31 located about 8 and 11 kpc from the nucleus (Hutchings et al. 1992). We therefore conclude that there is significant evidence for a deficiency of VSG in M31 compared to the Galaxy.

While the VSG abundance in the solar neighborhood appears to be typical for the Milky Way (DBP90; Boulanger & Pérault 1988), the occurrence of VSG-deficient regions in our Galaxy cannot be ruled out, especially at low illumination levels or outside the solar circle. Such occurrences would be similar to the strong variations in PAH abundance reported for pockets within molecular cloud complexes (Boulanger et al. 1990). On the other hand, the integrated colors of even the coldest galaxies remain higher in $R(60, 100)$ than all the model curves in Figure 3 (Helou et al. 1994), suggesting that as in M31, the mixing of emission from different heating environments masks the evidence. No statement can therefore be made about the fraction of galaxies with VSG deficiency as observed in M31, or about the relation between VSG and PAH abundances.

In view of this uncertainty, we can only speculate as to the causes of VSG deficiency, and its implications for the origin of VSG. If the deficiency is tied to the quiescence of M31 in terms of recent star formation (Walterbos 1987), it might indicate that VSG are not formed like large grains, and possibly the PAH molecules too (Mathis 1990), in the atmospheres of AGB stars, but rather require dense molecular clouds or supernova explosions as their birth places. Alternatively, VSG may require constant processing by supernova shock waves and/or strong UV radiation to avoid growing mantles and turning into large grains.

We are very grateful to E. Brinks for providing the H I map of M31, to B. Milliard for the UV (2000 Å) map, and to R. Walterbos for the optical photometry maps. Helpful discussions with C. Beichman and J. Fowler are acknowledged. A

large part of the work was done when C. X. held an Alexander von Humboldt Fellowship. This research is supported in part through the *IRAS* Extended Mission Program by the Jet Propulsion Laboratory, California Institute of Technology, under a contract with the National Aeronautics and Space Administration.

APPENDIX

SOURCES OF UNCERTAINTY OF M31 INTEGRATED FLUXES

In estimating uncertainties on the final M31 fluxes from this work (Table 1), we consider four sources of uncertainty.

A1. NOISE IN THE MAP

This is estimated from the dispersion in sky brightness away from sources, σ_0, and sets the minimum photometric uncertainty in the surface brightness measured in a pixel, and in the spatially integrated flux in an aperture. The dispersions measured on the raw HiRes maps within 10′ diameter apertures were 0.29, 0.27, 0.19, and 0.37 MJy sr^{-1} at 12, 25, 60, and 100 μm, respectively.

Spatial integrals suffer from a minimum uncertainty equal to $N_b^{1/2}\sigma_0$, where N_b is the number of independent resolution elements in the area over which the integration is taken.

A2. BACKGROUND SUBTRACTION

The relevant term here is departure from the assumption of a flat background due to structure in the foreground (Milky Way). We have tested for such departures by comparing the statistics of sky brightness in the 18 10′ diameter apertures used for background estimation. Each of these areas contains $N_b = 1232$, 778, 279, or 56 independent resolution elements at 12, 25, 60, 100 μm. The dispersion in the mean surface brightnesses of each area is larger than expected from $\sigma_0 N_b^{-1/2}$, the value expected if σ_0 was the only source of deviation from a flat background. We therefore derive a sky noise component with dispersion $\sigma_1 = 0.02$, 0.015, 0.07, and 0.2 MJy sr^{-1} on the scale of the test apertures. This will contribute $\sigma_1 N_c^{-1/2}$ to the integrated flux uncertainty, where N_c is the number of 10′ diameter apertures in the solid angle over which the flux is integrated.

The sky noise component characterized only by σ_1 always contributes less than the component due to σ_0 to the uncertainty on the total flux integral of M31. The *combined* terms amount to 45, 35, 15, and 13 Jy at 12, 25, 60, and 100 μm; these are in principle the only terms relevant to the comparison between HiRes and ISSA integrated fluxes. Formally, the larger discrepancy at 100 μm is probably due to the fact that sky structure (Milky Way cirrus) is more complex than the normal distribution representation adopted here.

A3. CALIBRATION

A3.1. *Absolute Calibration*

The absolute calibration of *IRAS* data is thought to be uncertain by 10% or less (*IRAS* Explanatory Supplement 1988). However, this is largely irrelevant to the results in this paper, because the discussion is confined to a comparison of *IRAS* colors. Moreover, the DBP90 model has been tied to the *IRAS* absolute calibration.

A3.2. *Local Deviations*

Local deviations of the calibration from the global *IRAS* calibration are small, typically $\leq 5\%$ (ISSA Explanatory Supplement 1994).

A3.3. *Calibration Uncertainties*

Calibration uncertainties associated with the variation of responsivity of *IRAS* detectors with "dwell time," or equivalently with source size arise because the HiRes maps we work with here use the very large source responsivity limit, whereas the M31 maps contain structure on various scales. The uncertainties should be bounded by the AC/DC responsivity ratio described in the *IRAS* Explanatory Supplement (1988, chap. IV).The ratio amounts to 0.78, 0.82, and 0.92 at 12, 25, and 60 μm, but was set to 1 at 100 μm because of the more complex behavior at this wavelength. From Figure IV.A.4.2 of the *IRAS* Explanatory Supplement, we estimate 20% as a reasonable upper limit to this source of uncertainty at 100 μm. We have adopted 11%, 9%, 4%, and 10% for the uncertainty at 12, 25, 60, and 100 μm.

A4. HiRes ARTIFACTS

Potential artifacts of HiRes for extended, low surface brightness sources have not been characterized. Point source photometry at relatively high signal-to-noise ratios is expected to be better than 20%. The uncertainties which appear in Table 1 do not include any term for such artifacts.

The contributions from §§ A1, A2, and A3.3 above are added in quadrature to yield the uncertainties listed in Table 1.

REFERENCES

Aumann, H. H., Fowler, J. W., & Melnyk, M. 1990, AJ, 99, 1674
Boulanger, F., Beichman, C., Désert, F. X., Helou, G., Pérault, M., & Ryter, C. 1988, ApJ, 332, 328
Boulanger, F., Falgarone, E., Puget, J.-L., & Helou, G. 1990, ApJ, 364, 136
Boulanger, F., & Pérault, M. 1988, ApJ, 330, 964
Castelaz, H. W., Sellgren, K., & Werner, M. W. 1987, ApJ, 313, 853
Cox, P., & Mezger, P. 1988, in Lecture Notes in Physics 297, Comets to Cosmology, ed. A. Lawrence (Heidelberg: Springer), 97
Désert, F. A., Boulanger, F., & Puget, J. L. 1990, A&A, 273, 215 (DBP90)
Draine, B. T., & Anderson, N. 1985, ApJ, 292, 494
Draine, B. T., & Lee, H. M. 1984, ApJ, 285, 89
Fowler, J. W., & Aumann, H. H. 1993, in Proc. of Workshop on Science with High Spatial Resolution Far-Infrared Data, in press
Helou, G. 1986, ApJ, 311, L33
———. 1989, in IAU Symp. 135, Interstellar Dust, ed. L. J. Allamandola & A. G. G. M. Tielens (Dordrecht: Kluwer), 285
Helou, G., Ryter, C., & Soifer, B. T. 1991, ApJ, 376, 505
Helou, G., et al. 1994, in preparation
Hutchings, J. B., et al. 1992, ApJ, 400, L35
Léger, A., & Puget, J. L. 1984, A&A, 137, L5
Mathis, J. S. 1990, ARA&A, 28, 37
Milliard, B. 1984, Ph.D. thesis, Université de Provence Aix – Marseille I
Pérault, M., Boulanger, F., Puget, J. L., & Falgarone, E. 1988, unpublished
Puget, J. L., & Léger, A. 1989, ARA&A, 27, 161
Rice, W. 1993, AJ, 105, 67
Rice, W., Boulanger, F., Viallefond, F., Soifer, B. T., & Freedman, W. L. 1990, ApJ, 358, 418
Rice, W., Lonsdale, C. J., Soifer, B. T., Neugebauer, G., Kopen, E. L., Lloyd, L. A., de Jong, T., & Habing, H. J. 1988, ApJS, 68, 91
Sauvage, M., Thuan, T. X., & Vigroux, L. 1990, A&A, 237, 296
Sellgren, K. 1984, ApJ, 277, 623
Soifer, B. T., Rice, W., Mould, J. R., Gillett, F. C., Rowan-Robinson, M., & Habing, H. 1986, ApJ, 304, 651
Walterbos, R. A. M. 1987, in Galactic and Extragalactic Star Formation, ed. R. E. Pudritz & M. Fich (Dordrecht: Kluwer), 361
Walterbos, R. A. M., & Kennicutt, R. 1988, A&A, 198, 61
Walterbos, R. A. M., & Schwering, P. B. W. 1987, A&A, 180, 27
Xu, C., & De Zotti, G. 1989, A&A, 225, 12
Xu, C., & Helou, G. 1994, in preparation
Xu, C., Klein, U., Meinert, D., Wielebinski, R., & Haynes, R. F. 1992, A&A, 257, 47